DOI: https://doi.org/10.3329/jnujles.v10i2.85255



JnUJLES

Research Article

URBAN GROWTH-DRIVEN LAND USE AND CLIMATE DYNAMICS: ASSESSING CHANGES IN DHAKA CITY (1990–2022)

Md. Asraf Uddin^{1*}, Masuda Sultana², Neegar Sultana¹, and Md. Kamrul Islam²

¹ Department of Geography and Environment, Jagannath University, Dhaka-1100, Bangladesh.

Received: 05 February 2025,

Accepted: 03 June 2025

ABSTRACT

Since 1990, Dhaka has experienced rapid, unplanned urban expansion, profoundly altering land-use patterns and intensifying local climate extremes in one of the world's most densely populated megacities. This study aims to quantify three decades of land use and land cover (LULC) changes and evaluate their associated impacts on land surface temperature (LST), near-surface air temperature, and rainfall, with a view to informing climate-resilient urban planning. Landsat 5 TM (1990) and Landsat 9 OLI-2/TIRS-2 (2022) imagery were analyzed using ArcGIS and ERDAS Imagine to classify built-up areas, vegetation, bare land, and water, achieving high accuracy ($\kappa = 0.93$). LST was estimated using radiometric calibration, NDVI-based emissivity correction, and the mono-window algorithm, while long-term climate data from the Bangladesh Meteorological Department supported trend analysis. Findings reveal a 41.15% increase in built-up area, largely at the expense of vegetation (-31.02%), resulting in a 4.87 °C rise in peak LST and a 71 mm increase in annual rainfall. Strong positive correlations ($|r| \ge 0.99$) show that each 1% gain in built-up land adds approximately 0.12 °C to LST and enhances convective precipitation, whereas vegetation loss exerts a cooling and drying effect. These dynamics are exacerbating urban-heat-island intensity, disrupting seasonal rainfall, and increasing flash-flood and health risks. To counteract these effects, the study recommends vertical urban densification, conservation of wetlands and green belts, and integration of green-blue infrastructure alongside high-resolution remote sensing and climate modeling for adaptive urban policy and planning.

Keywords: urban expansion, land use and land cover change (LULC), urban heat island (UHI), land surface temperature (LST), climate-resilient urban planning

Introduction

Climate change is widely regarded as a global problem (Abbas *et al.*, 2023; Biswas, 2023; Moshou and Drinia, 2023; Swinburn *et al.*, 2022). Although climate change is treated as a global issue, many scholars now argue that it should be viewed as a multi-level problem requiring

_

²GIS Analyst, Institute of Water Modelling (IWM), Dhaka, Bangladesh.

^{*}Correspondence: masrafuddin.85@gmail.com

localized and regional responses (Bulkeley and Newell, 2023). Human activities have significantly altered the environment for thousands of years, with extensive land use and land cover changes (LULCC) playing a crucial role in influencing atmospheric temperature trends (Mahmood *et al.*, 2010). Hence, land use and land cover change analysis are vital for assessing global environmental changes across various spatial and temporal scales (Hurtt *et al.*, 2021; Lambin, 1997).

Urban growth-driven land use and land cover changes are among the most significant anthropogenic factors influencing weather patterns, contributing to increased greenhouse gas emissions worldwide (Liu et al., 2019). Such urbanization leads to substantial LULC changes, significantly affecting land surface temperature (LST) in rapidly growing megacities (Kafy et al., 2021). The combined effects of greenhouse gas emissions and land use changes are significant drivers of climate change, often leading to increases in daily mean surface air temperatures (Yang et al., 2009). Furthermore, Recent empirical studies show rapid LULC change in developing regions. For instance, Tahir et al. (2025) documented a 359.8 km² urban expansion and 198.7 km² vegetation loss in Lahore (1994–2024). Similarly, Gabisa et al. (2025) reported that in Burayu sub-city cropland dropped from 51.2 % to 30.3 %, forest from 32.9 % to 15 %, and settlement grew from 2.5 % to 46.9 % (1993–2023). These trends reinforce the view that anthropogenic LULC changes are occurring faster in developing countries vs developed nations. Large-scale land use and cover changes, particularly in developed countries with rapid urbanization trends, have become a pressing concern as urban expansion drives environmental changes across multiple scales (Dewan et al., 2012).

Land-use land-cover (LULC) changes significantly influence local climate dynamics (Ding and Shi, 2013). Bangladesh is one of the most climate-vulnerable countries in the world (World Bank, 2022). In recent years, the country has undergone substantial land use and land cover changes (LULCC) (Xu et al., 2020). Dhaka, the capital of Bangladesh, has experienced rapid urban growth over the last few decades, resulting in numerous adverse environmental impacts (Dewan et al., 2012). Land use changes driven by urbanization, including deforestation and rapid population growth, have led to unpredictable heavy rainfall and rising temperatures (Thapa, 2021). These changes highlight the need for administrative interventions to mitigate their effects on the livelihoods of urban populations. Geographic Information Systems (GIS) and remote sensing (RS) are cost-effective tools for analyzing the spatial and temporal dynamics of land use and land cover (LULC) changes (Bikis et al., 2025; Halder et al., 2025; Mashala et al., 2023). Geospatial and statistical analyses also support urban land use planning programs.

Urbanization predominantly reflects land-use changes and is widely recognized as a primary driver of climate and ecological changes (Ding and Shi, 2013). Rising sea levels, floods, and intensifying cyclones further exacerbate Bangladesh's vulnerability to climate change (IPCC). Urbanization has significantly contributed to these issues by replacing vegetation and bare land with built-up areas, leading to remarkable increases in land surface temperature (LST) (Gazi *et al.*, 2021). The construction of urban infrastructure for housing, transportation, and industry has disrupted the surface energy balance, further elevating LST (Imran *et al.*, 2021). This rise in LST

has adversely impacted urban biodiversity, ecosystems, and public health (Kafy et al., 2021).

Urban growth induced LULC changes are closely linked to LST fluctuations (Rahman *et al.*, 2022). The major districts of Bangladesh, with their large population bases, lack adequate resources to address the effects of rapid urbanization. Consequently, urban temperature increases directly and indirectly affect these populations (Rahman *et al.*, 2022). Urban areas not only alter weather patterns but also influence water runoff dynamics. A strong relationship exists between LST and near-surface air temperature (Tair), though the two have distinct physical characteristics and responses to atmospheric conditions (Mutibwa *et al.*, 2015). Urbanization-driven LULC changes also affect urban microclimates and can significantly influence precipitation patterns (Pathirana *et al.*, 2014).

This study aims to assess the spatiotemporal relationship between urban land-use/land-cover (LULC) changes and climate dynamics in Dhaka City from 1990 to 2022. It focuses on classifying LULC using multi-temporal Landsat imagery and analyzing changes in land surface temperature (LST), air temperature, and rainfall. The objectives include exploring how urban expansion influences local climate patterns and offering evidence-based recommendations for sustainable urban planning and climate resilience.

Materials and Methods

Study area

This study was conducted in the central region of Bangladesh. Dhaka, the capital city, is located at approximately 23°46'48"N latitude and 90°25'36"E longitude (*Figure 1*) on the northeastern banks of the Buriganga River. The Balu River borders the city to the east, Tongi Khal to the north, and the Turag River to the west. Dhaka lies in the lower reaches of the Ganges Delta and spans a total area of 306.4 km² (Bangladesh Bureau of Statistics [BBS], 2023; Hossain *et al.*, 2023; Abdullah *et al.*, 2021; Nowreen *et al.*, 2021). The districts of Gazipur, Tangail, Munshiganj, Rajbari, Narayanganj, and Manikganj surround Dhaka District.

As the country's most populous and urbanized city, Dhaka has undergone significant land use changes impacting its climate. It is widely recognized as the world's most densely populated built-up urban area (Demographia, 2023). Dhaka Metropolitan City comprises 41 thanas, 81 wards, 59 unions, and 841 mahallas and mouzas. In 2011, the city was administratively divided into two municipal corporations: Dhaka South City Corporation (DSCC) and Dhaka North City Corporation (DNCC).

Dhaka is the largest city in Bangladesh and ranks among the top densely populated cities worldwide. Dhaka is currently the fourth largest and among the most densely populated cities in the world, with approximately 10.3 million residents in its two city corporations (BBS, 2023) and a metropolitan population exceeding 24.6 million in 2025 (UN DESA, 2024; World Population Review, 2025). Dhaka's terrain is predominantly flat, with elevations generally ranging from 1 m to 14 m above mean sea level (Sayed and Haruyama, 2016). Consistent with recent urban climatology research, Dhaka is classified as a tropical wet and dry (Aw) climate under the Köppen system, indicating a distinctly seasonal rainfall pattern with pronounced dry winters (Islam and Hasan, 2023; Tabassum *et al.*, 2024).

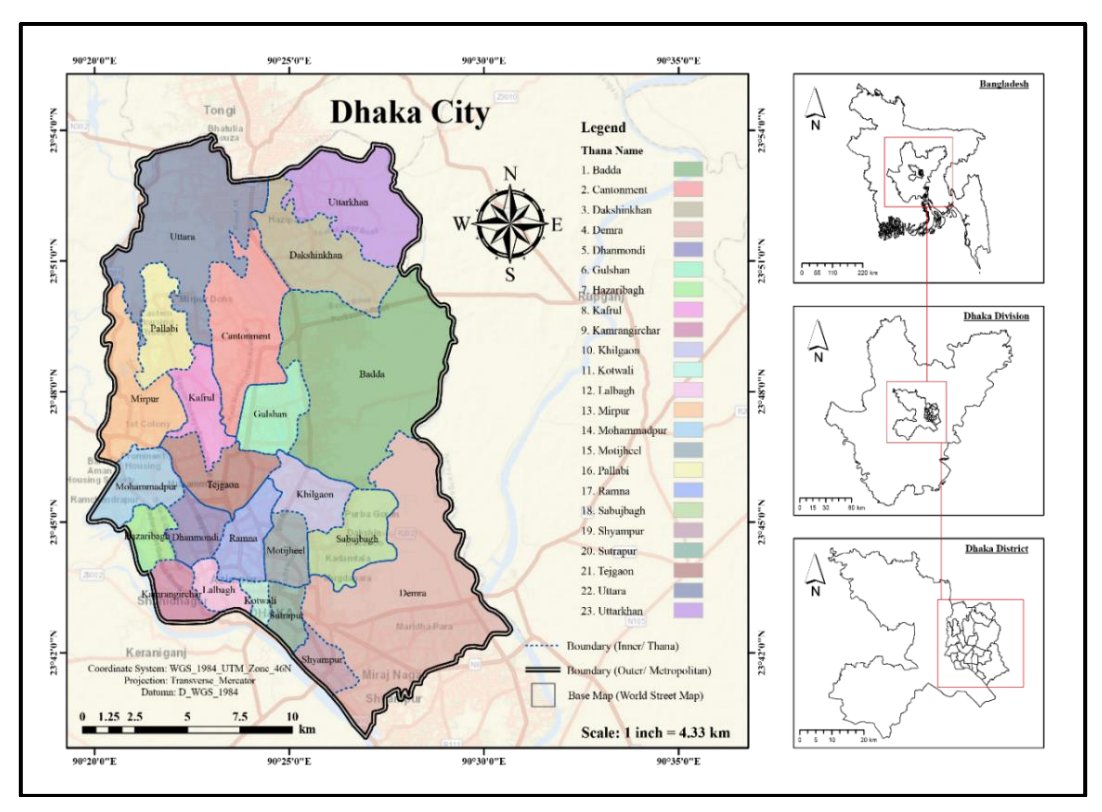


Figure 1: Location of the study area (Dhaka City, Bangladesh), Source: Author 2024

Data Source

For this study, two multi-date Landsat image series—Landsat 5 TM (1990) and Landsat 9 OLI-2/TIRS-2 (2022)—were utilized to analyze land surface temperature (LST) and land use/land cover (LULC) changes. The LULC analysis was performed using images with a 30-meter spatial resolution, while LST interpretation was conducted using a resolution of 120 meters for Landsat 5 and 100 meters for Landsat 9. All geospatial data were processed using the Universal Transverse Mercator (UTM) projection in Zone 46N, based on the World Geodetic System 1984 (WGS84) ellipsoid datum.

The Landsat images were downloaded from the United States Geological Survey (USGS) website. Satellite imagery was effectively used to identify the study area. A shape file of Dhaka was also obtained from the DIVA-GIS website to mask the study area during digital image processing. Landsat 5 TM images were analyzed for 1990, while Landsat 9 OLI-2/TIRS-2 images were analyzed for 2022, covering both LULC and LST assessments. Detailed information about the satellite imagery used in the study is summarized in Table 1 and Table 2. Additionally, rainfall and air temperature data were collected from the Bangladesh Meteorological Department to analyze rainfall and air temperature changes over the 32-year study period, spanning 1990 to 2022 for rainfall and 1990 to 2022 for air temperature.

Table 1. Characteristics of satellite images LULC analysi

Satellite sensors	Date of acquisition	Row/Path	Resolution (Meters)	Projection		
Landsat 5 TM	1990-04-29	044/137	30	UTM/WGS 84		
Landsat 9 OLI-2/TIRS-2	2022-11-07	044/137	30	UTM/WGS 84		

Source: United States Geological Survey (USGS).

Table 1. Characteristics of satellite images LST analysis

Satellite sensors	Date of acquisition	Row/Path	Resolution (Meters)	Projection		
Landsat 5 TM	1990-04-29	044/137	120	UTM/WGS 84		
Landsat 9 OLI-2/TIRS-2	2022-11-07	044/137	100	UTM/WGS 84		

Source: United States Geological Survey (USGS, 2024)

ArcGIS 10.5 and ERDAS IMAGINE 15 were used to perform all image processing tasks and generate LULC and LST maps for 1990 and 2022. Additionally, Microsoft Excel was applied to export areal information and create graphs depicting land use and land cover changes within the study area.

Image Processing

Various data processing techniques were employed to analyze different data types for this research. Using GIS, digital image processing techniques were applied to measure LULC and LST. The area of interest (AOI) was delineated using a polygon shape file of Dhaka city, separated from the Upazila shape file of Bangladesh using the dissolve tool in ArcGIS 10.5. Subsequently, the study area was extracted from the satellite images using the Clip tool in the ArcGIS toolbox. Additionally, statistical methods were utilized to process rainfall and air temperature data collected from the Bangladesh Meteorological Department. All the data were processed and edited, and graphs were generated using Microsoft Excel for further analysis.

Land Use Land Cover Assessment

The Landsat satellite images collected from USGS Earth Explorer consist of multiple spectral bands. Color composite images (RGB) were created by layer stacking bands 321 for Landsat 5 and 432 for Landsat 9 using ERDAS IMAGINE 15. A supervised image classification method was applied to derive the land use/land cover (LULC) categories from the Landsat 9 image, as it relies on prior knowledge of the study area. For Landsat 5, a hybrid image classification approach (combining unsupervised and supervised methods) was adopted, as exact training data for the study area were unavailable.

All images were analyzed based on their spectral and spatial profiles of digital number (DN) values. Training sites for classification were developed using reference data and ancillary information obtained from various sources, along with natural color composite bands. The acquired satellite images from 1990 and 2022 were classified into four broad land cover types, as summarized in Table 3.

Table 3. Land Use/Land Cover (LULC) Types

Land Use/Cover Types	Description
Built-up Area	Includes all infrastructure such as residential, commercial, mixed-use, industrial areas, villages, settlements, road networks, pavements, and other man-made structures.
Water Body	Encompasses rivers, permanent open water, lakes, ponds, canals, permanent/seasonal wetlands, low-lying areas, marshy lands, and swamps.
Vegetation	Covers trees, natural vegetation, mixed forests, gardens, parks, playgrounds, grasslands, vegetated lands, agricultural lands, and crop fields.
Bare Land	Includes fallow land, earth and sand landfills, construction sites, developed land, excavation sites, open spaces, bare soils, and other remaining land cover types.

Source: Author (2024)

Hybrid and Supervised Image Classification Techniques

Hybrid image classification techniques were employed to process the Landsat five image from 1990 into four land cover classes. All classification and area calculation tasks were performed using ERDAS IMAGINE 15 and ArcGIS 10.5 software. A hybrid classification approach (combining unsupervised and supervised methods) was adopted to classify the images into discrete land use/cover categories. Initially, the Landsat 5 image was classified using the K-means clustering technique, with a maximum of 10 iterations in the unsupervised classification procedure. The resulting clusters were evaluated using histogram plots. Similar clusters were identified and merged into unified classes using the color recode tool in ERDAS IMAGINE. These unified classes were assigned to one of the four land use/cover types: bare land, built-up area, vegetation, or water bodies. This process was repeated for all four classes. Finally, the classified raster images were converted into vector polygon shapes using the raster-to-polygon tool in ERDAS IMAGINE.

The symbology of the layers was updated in ArcGIS to assign class names by adding a new field labeled "Class Name" to the attribute table. Another field, labeled "Area," was added to calculate the area of different polygons for each class using the "Calculate Geometry" tool in ArcGIS.

For the Landsat 9 image from 2022, supervised image classification techniques were applied. All tasks were performed using ERDAS IMAGINE 15 software. Initially, 50 signature polygons were created for each land use/cover type feature and merged into unified classes. This process was repeated for the four land cover types, resulting in 200 signatures. The spectral and spatial profiles of digital numbers (DNs) were analyzed to differentiate LULC categories (Dewan and Corner, 2012). A final signature file was created for classification, and four distinct land cover classes were exported with unique colors and names to represent the features.

A maximum likelihood algorithm was used to complete the supervised classification process. This algorithm calculated the probability of each pixel belonging to a specific class based on its attribute values (ArcGIS, 2012). This method reassigned Isolated pixels to the most common neighboring class, reducing noise (Civco, 1993). The generalized classes were reclassified to produce the final land cover map.

Finally, to calculate the area of the different land cover classes and detect changes, raster-to-polygon conversion tools were used in ERDAS IMAGINE. The area of each class was calculated in ArcGIS by adding a new field named "Area" in the attribute table and using the "Calculate Geometry" tool.

Accuracy Assessment of LULC

Accuracy assessment is a critical step in any classification project, as the reliability and acceptability of image classification depend on its accuracy level (Islam *et al.*, 2021). To evaluate the accuracy of the classified land cover images, ground point values were selected automatically using tools in ArcGIS 10.5 software. Randomly distributed ground points were chosen for the confusion matrices from the classified images for 1990 and 2022.

The confusion matrix method was employed for accuracy assessment. User accuracy is the ratio of correctly classified units in a given class to the total number of units classified in that class. In contrast, producer accuracy is the ratio of correctly classified units in a class to the total number of reference units for that class (Bradley, 2009). Following established definitions (Congalton and Green, 1999; Lu and Weng, 2007;), recent studies continue to use overall accuracy (OA)—the ratio of correctly classified cases to total cases across all classes (Sun and Liu, 2023). For instance, a U-Net deep-learning approach in South Korea achieved 90.3 % OA (Sim et al., 2024), while evaluations of classifiers like Random Forest and SVM report OA values > 0.91 (Kumar et al., 2023), Global mapping exercises in Siberia yield OAs around 85 % (Tang et al., 2024), and product comparisons in Romania show OA spans 67-85 % depending on dataset (Ionescu and Popescu, 2024). This study generated 100 random sampling points for each image using the "Create Accuracy Assessment Points" tool in the ArcGIS Spatial Analyst Toolbox. High-resolution imagery from Google Earth TM was used as reference data to validate the classified datasets for 1990 and 2022. Additionally, a non-parametric Kappa test was conducted to measure classification accuracy. This test considers both the diagonal elements of the confusion matrix and all other elements, providing a robust measure of agreement (Rosen field and Fitzpatrick-Lins, 1986). The confusion matrices of the classified images were calculated and verified using the "Compute Confusion Matrix" tool in ArcGIS software, ensuring comprehensive accuracy assessment.

Land Surface Temperature Measurement

Land Surface Temperature (LST) represents the radiative skin temperature of the land, calculated from the emission of thermal radiance. LST is determined by the interaction of incoming solar energy with the ground surface or the canopy surface in vegetated areas, where this energy is absorbed and subsequently re-emitted as heat.

This study used reflective bands from Landsat 5 (1990) and Landsat 9 (2022) satellite images for image processing, transformation, and analysis to evaluate changes in LST across Dhaka city,

Bangladesh. Geographic Information System (GIS) tools and advanced digital image processing techniques were applied to carry out the methodology effectively. Spectral bands were selected and tailored for each year's satellite imagery to meet the specific analytical requirements of the study.

Calculating the LST of Landsat 5

To calculate Land Surface Temperature (LST) from Landsat 5 TM data, a two-step process was implemented to retrieve brightness temperature.

Step 1. Conversion of DN to Radiance: The first step involved converting the Digital Numbers (DN) of Thermal Band 6 into radiance using the Eq1.

$$L_{\lambda} = \left(\frac{LMAX_{\lambda} - LMIN_{\lambda}}{QCALMAX - QCALMIN}\right) \times (QCAL - QCALMIN) + LMIN_{\lambda} \qquad(1)$$

Where L_{λ} is Spectral radiance,

QCAL = Quantized calibrated pixel value in DN

 $LMAX_{\lambda} = Spectral\ radiance\ scaled\ to\ QCALMAX\ in\ (Watts/(m^2*sr*\mu m))$

 $LMIN_{\lambda} = Spectral\ radiance\ scaled\ to\ QCALMIN\ in\ (Watts / (m^2*sr*\mu m))$

OCALMIN = Minimum quantized calibrated pixel value (corresponding to LMINA) in DN

 $QCALMAX = Maximum \ quantized \ calibrated \ pixel \ value \ (corresponding \ to \ LMAX,) \ in DN=255.$

Step 2. Converting Radiance to Brightness Temperature (BT): The second step calculated the effective at-satellite temperature using Eq. 2.

$$T = \frac{\kappa_2}{\ln\left(\frac{\kappa_1}{L_\lambda} + 1\right)} \tag{2}$$

WhereT = Effective at-satellite temperature in Kelvin

 $K_2 = Calibration constant 2$

 $K_1 = Calibration constant 1$

 L_{λ} = Spectral radiance in (Watts / (m^{2*} sr* μm))

ln = Natural logarithm

Step 3. Conversion of Kelvin to Celsius: The temperature in Kelvin was then converted to degrees Celsius using the Eq. 3.

$$C = T - 273.15$$
(3)

3.7 Calculating the LST of Landsat 9

A similar multi-step approach was used to calculate LST from Landsat 9 OLI/TIRS-2 data, with additional band-specific parameters for the thermal infrared Band 10.

Step 1. Conversion to TOA Radiance: Thermal Infra-Red Digital Numbers (DN) were converted to Top of Atmosphere (TOA) spectral radiance using Eq. 4.

Where L_{λ} is the TOA Spectral Radiance (Watts/ (m2 * sr * μ m)), M_L represents the band-specific multiplicative rescaling factor, Q_{cal} is the Band 10 image, and A_L is the band-specific additive rescaling factor.

Step 2. Conversion to TOA Brightness Temperature: TOA spectral radiance was then converted to TOA brightness temperature using the Eq. 5.

$$BT = \frac{\kappa_2}{\ln\left(\frac{\kappa_1}{L_{\lambda}} + 1\right)} - 273.15 \tag{5}$$

Where, BT is the Top of Atmosphere Brightness Temperature in °C,

 K_1 = Band-specific thermal conversion constant from the metadata,

(K_1 is constant band x, where x is the thermal band number).

 K_2 = Band-specific thermal conversion constant from the metadata,

(K_2 is constant band x, where x is the thermal band number).

 $L = TOA(Top \ of \ Atmosphere).$

Therefore, to obtain the results in Celsius, the radiant temperature is adjusted by adding the absolute zero (approximately -273.15°C).

Table 4. Metadata of the satellite images

Therm	al constant, Band 10			
K_1	1321.08			
K ₂	777.89			
Rescaling factor, Band 10				
$\mathrm{M_L}$	0.000342			
$A_{\rm L}$	0.1			
	(Source: USGS, 2024)			

the metadata (table 4) is sourced from the United States Geological Survey (USGS), which provides calibration constants and rescaling factors in the metadata files for satellite imagery, such as Landsat products.

Step 3: Calculating Normalized Differential Vegetation Index (NDVI)

The Normalized Differential Vegetation Index (NDVI) is a standardized index for vegetation that is computed using Near Infra-red (Band 5) and Red (Band 4) bands.

$$NDVI = (NIR - RED) / (NIR + RED) \qquad \dots (6)$$

Where, RED = DN values from the RED Band, and NIR= DN values from Near-Infrared Band. Step 4: Calculating the Proportion of Vegetation

The proportion of Vegetation (P_V) is calculated using the following equation. A method for calculating P_V suggests using the NDVI values for vegetation and soil $(NDVI_V = 0.5)$ and

NDVIs = 0.2) to apply in global conditions:

$$P_{V} = ((NDVI - NDVI_{S} / NDVI_{V} - NDVI_{S}))^{2} \qquad(7)$$

Here,

$$P_V = [(NDVI - NDVI min) / (NDVI max - NDVI min)]^2$$

Where, P_V = Proportion of Vegetation, NDVI = DN values from NDVI Image, NDVI min = Minimum DN values from NDVI Image, and NDVI max = Maximum DN values from NDVI Image.

Step 5: Calculating Land Surface Emissivity (LSE):

The Land surface emissivity (LSE) is the average emissivity of an element of the Earth surface calculated from NDVI values. The determination of the ground emissivity is calculated conditionally as suggested in:

$$\varepsilon = 0.004 * P_V + 0.986$$
(8)

Where, $\varepsilon = \text{Land Surface Emissivity}$, and PV= Proportion of Vegetation.

Step 6: Land Surface Temperature (LST):

The Land Surface Temperature (LST) is the radioactive temperature which calculated by using top of atmosphere brightness temperature, Land Surface Emissivity and Wavelength of emitted radiance.

LST =
$$(BT / (1 + (W * BT / 1.4388) * ln(\epsilon)))$$
(9)

Where, BT = Top of Atmosphere Brightness Temperature (°C), W= Wavelength of Emitted Radiance, and ε = Land Surface Emissivity.

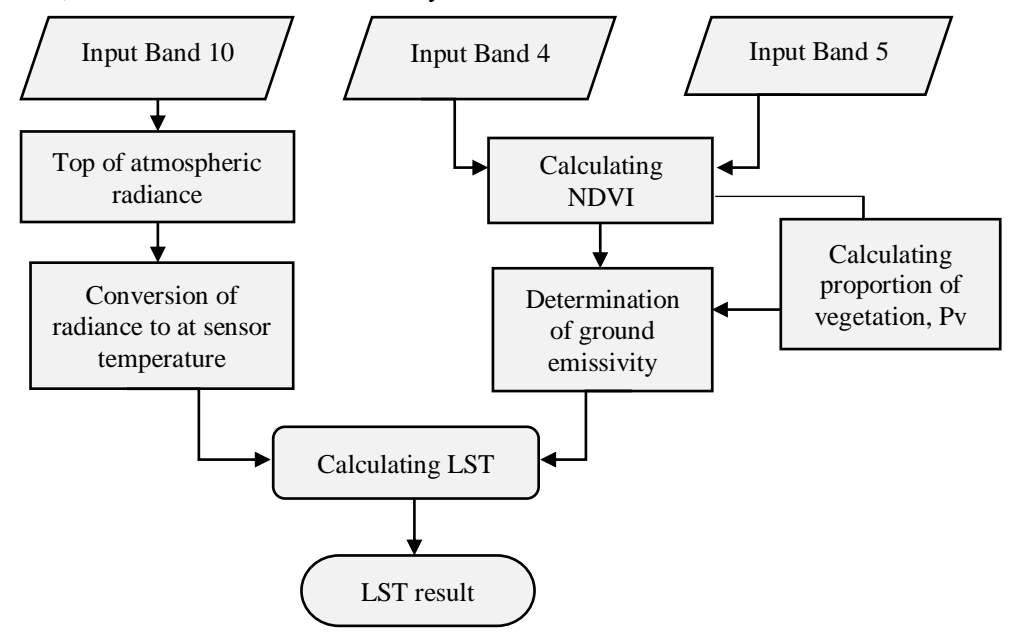


Figure 2 interprets the whole methods of land surface temperature generating process.

Figure 2:Flowchart for LST retrieval of Landsat 9 (Source: Author, 2024).

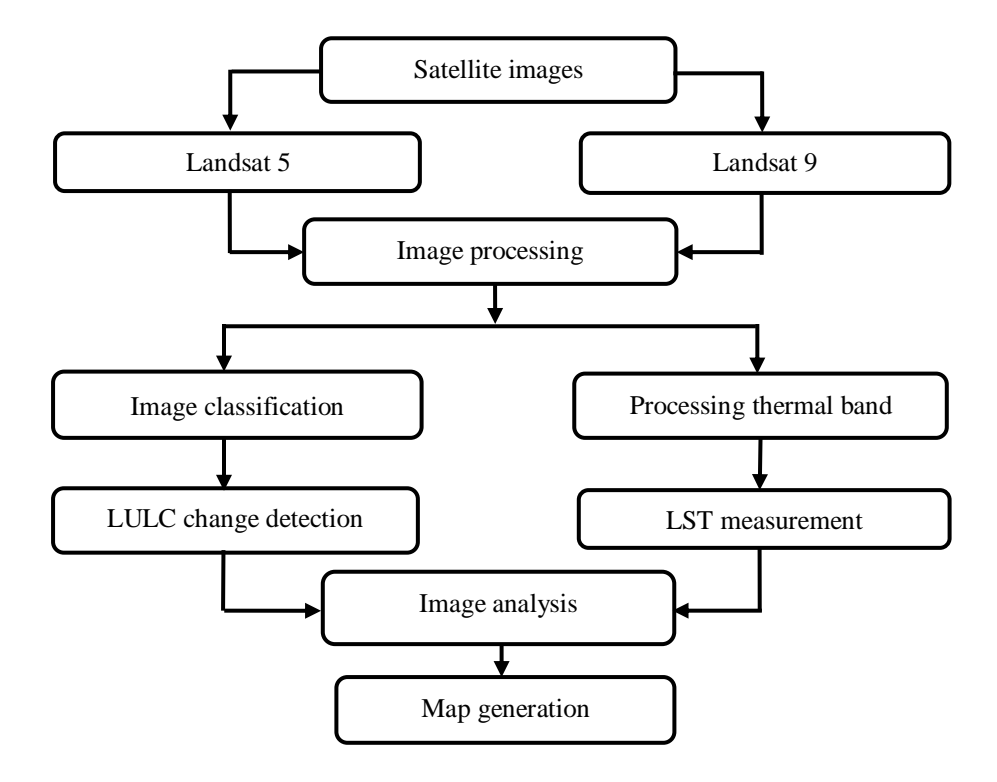


Figure 3: Methodological flowchart (Source: Author, 2024).

Figure 3 illustrates the complete methodology used in this study. Two types of satellite images were utilized, both of which were obtained from the USGS website.

Results and Discussion

Land Use Land Cover Change Analysis

LULC changes were identified using Landsat 5 and Landsat 9 images from 1990 and 2022, respectively, by creating generalized LULC maps. The LULC maps were generated using image classification techniques for each year's imagery. Subsequently, the areas of the four land cover classes were calculated for the study area. Changes in LULC were analyzed by comparing the maps from 1990 and 2022. The land cover change patterns during this period are illustrated in Figure 4.

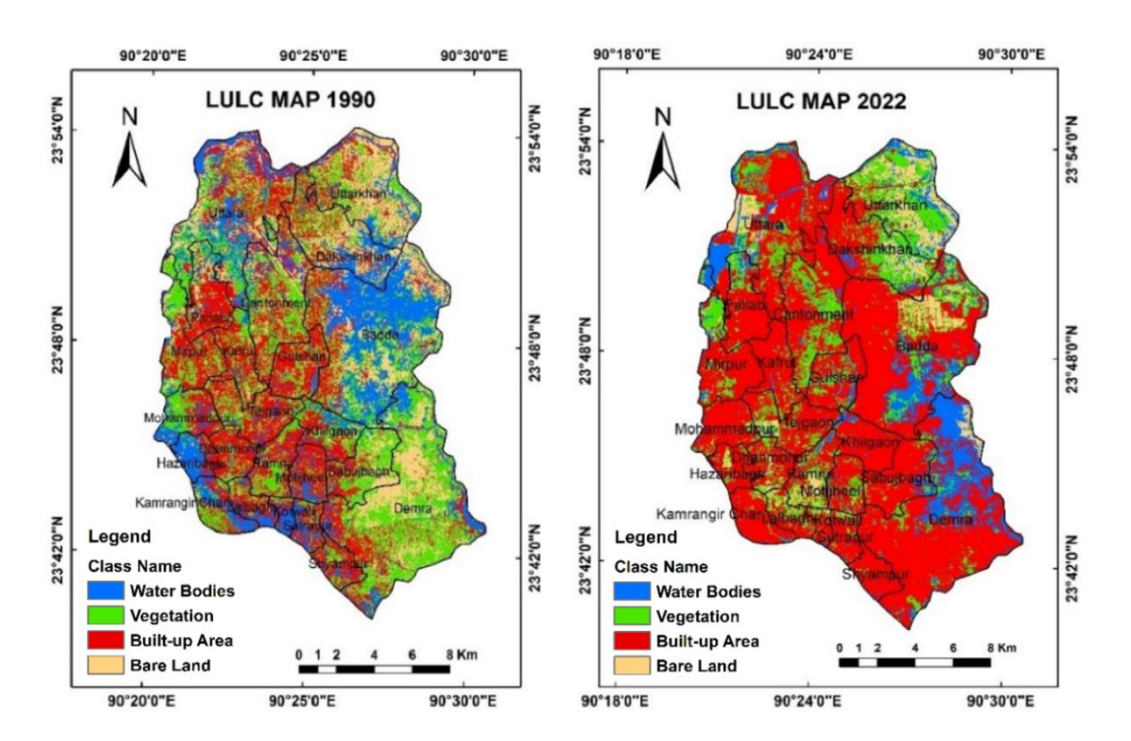


Figure 4.Land use land cover map of 1990 and 2022; Source: Prepared by Authors, 2024

Figure 4 depicts the land use/land cover (LULC) of Dhaka Metropolitan Area for 1990 and 2022, divided into four land cover classes: bare land, built-up area, vegetation, and waterbodies. The map of 1990 shows a significant presence of waterbodies in the middle east (Badda Thana), the southwest, and the upper north side of the city. The built-up areas were concentrated in the central and western parts, while most bare land was located in the north-east and south-east of the city. Vegetation was scattered throughout the city, indicating a more balanced distribution. Notably, most waterbodies and built-up areas were found in the Dhaka North City Corporation area, whereas bare land was predominantly observed in the South City Corporation area.

In contrast, the 2022 land use/cover map reveals that built-up areas dominated most parts of the city, both in the North and South City Corporation areas. Waterbodies within the South City Corporation were primarily located in the south-east. Vegetation was concentrated in the northeast and dispersed sporadically across the central parts of both city corporations. Only a small portion of bare land remained, mainly in the northeastern part of the city.

A comparison of the 1990 and 2022 maps indicates a significant expansion of built-up areas, with a corresponding reduction in bare land, vegetation, and waterbodies. Most waterbodies in the middle east were filled with soil and converted into built-up areas and bare land, except in Uttar khan Thana, which retained some of its original land cover. This transformation underscores the impact of human-induced activities driving the continuous urbanization of Dhaka city. The data for the areas of each land use/cover class are presented in the Table 5.

Table 5. LULC classes area of each category and percentage

]	1990	2		
LULC Classes	Area (ha)	Percentage (%)	Area (ha)	Percentage (%)	Changes (%)
Bare land	4232.5	13.99	2412.7	7.93	-6.06
Built-up area	6732	22.25	19,289.6	63.4	+ 41.15
Vegetation	15,737	52.02	6389.1	21	-31.02
Waterbodies	3548	11.74	2334.78	7.67	-4.07
Total	30249.5	100.0	30426.2	100.0	

(Source: Authors, 2024)

Table 5: LULC changes in Dhaka from 1990 to 2022 across four categories: bare land, built-up area, vegetation, and waterbodies. In 1990, vegetation was the dominant category, covering 15,737 hectares and accounting for 52.02% of the total area. Built-up areas occupied 6,732 hectares (22.25%), making them the second-largest category. Bare land covered 4,232.5 hectares (13.99%), while waterbodies accounted for 3,548 hectares (11.74%).

By 2022, built-up areas experienced a dramatic increase to 19,289.6 hectares, comprising 63.4% of the total area—a rise of 41.15%. Vegetation saw a significant decline, dropping to 6,389.1 hectares (21%), a reduction of 31.02%. Bare land also decreased to 2,412.7 hectares (7.93%), a loss of 6.06%. Waterbodies exhibited the most minor decrease, reducing to 2,334.78 hectares (7.67%), a decline of 4.07%. The total area remained consistent at approximately 30,000 hectares, indicating that these changes resulted from land use conversions within the existing area. These trends reflect rapid urbanization, with built-up areas expanding at the expense of vegetation, bare land, and waterbodies, underscoring significant environmental impacts over the 32 years.

Accuracy of Classified Images

The accuracy of the derived land cover maps from satellite data was assessed using error matrices. These matrices summarized the classification accuracy for the two years of land use/cover data. The confusion matrices for individual accuracy assessments of the classified images are presented in Table 6.

Table 6. Confusion matrix for the classified images using Google Earth Pro

	19	990	20)22		
LULC Classes	User accuracy	Producer	User accuracy	Producer		
	(%)	accuracy (%)	(%)	accuracy (%)		
Bare land	82.14	82.14	88.89	100		
Built-up area	78.95	93.75	97.06	94.29		
Vegetation	100	87.5	88.24	100		
Waterbodies	84.38	84.38	100	91.18		
Overall accuracy		86.37 93.55				
Kappa coefficient	t	0.81	0.	93		
			/Car			

(Source: Authors, 2024)

Table 6 presents the user accuracy and producer accuracy for each LULC class in 1990 and 2022, along with the overall accuracy and Kappa coefficient. User accuracy refers to the likelihood that a pixel classified into a specific category belongs to that category, while producer accuracy measures the probability that a reference pixel is correctly classified into its true category.

For bare land, user accuracy improved from 82.14% in 1990 to 88.89% in 2022, while producer accuracy increased significantly from 82.14% to 100%. Built-up areas exhibited substantial improvement, with user accuracy rising from 78.95% in 1990 to 97.06% in 2022 and producer accuracy increasing slightly from 93.75% to 94.29%. Vegetation achieved 100% user accuracy in 1990, which decreased to 88.24% in 2022, but producer accuracy improved from 87.5% to 100%. Waterbodies experienced a marked improvement, with user accuracy increasing from 84.38% in 1990 to 100% in 2022, while producer accuracy rose from 84.38% to 91.18%.

The overall accuracy of the classification increased from 86.37% in 1990 to 93.55% in 2022, demonstrating enhanced reliability in the classification process. The Kappa coefficient, a statistical measure of classification agreement, improved from 0.81 in 1990 to 0.93 in 2022, indicating a higher level of classification consistency. These improvements underscore advancements in classification techniques and the quality of input data over time. The elevated overall accuracy and Kappa coefficient values demonstrate the reliability and robustness of the classified maps for assessing LULC changes in Dhaka.

Land Surface Temperature Dynamics

The dynamics of land surface temperature (LST) from 1990 to 2022 are illustrated in Figure 5. The LST maps depict the high and low values of LST in degrees Celsius. Both the highest and lowest LST values increased during this period. In 1990, the maximum LST was 32.46°C, which rose by 4.87°C to 37.33°C in 2022. Similarly, the minimum LST 1990 was 21.5°C, which increased by 2.95°C to 24.45°C in 2022.

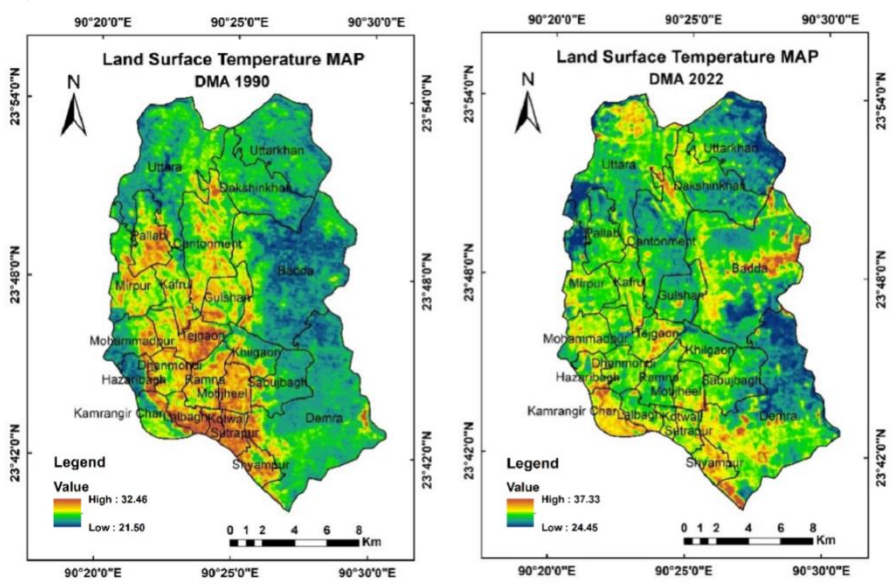


Figure 5. Land surface temperature from 1990 to 2022 (Source: Authors, 2024).

In 1990, the highest LST values were observed in the western part of the city, while the lowest values were recorded in the eastern areas. By 2022, the highest LST values were concentrated near the city's boundaries, while the lowest values remained distributed around the outskirts. The trends in LST changes are further detailed in the graphs presented in Figure 6.

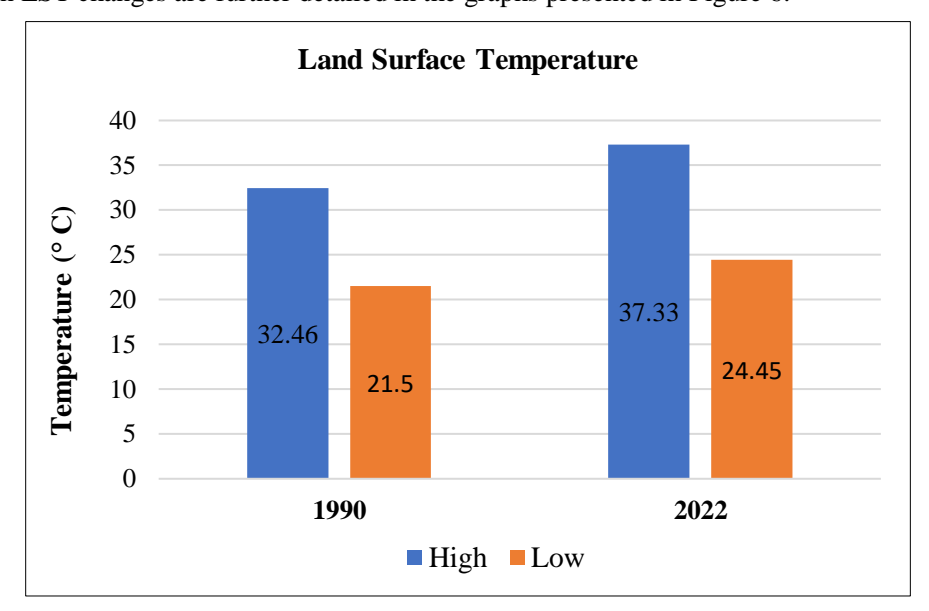


Figure 6. Land surface temperature changes between 1990 and 2022 (Source: Authors, 2024).

Comparison Between LULC and LST Maps

An analysis of LULC and land surface temperature (LST) maps reveals distinct temperature distribution patterns. In 1990, the highest LST values were observed in the built-up areas of Dhaka, while the lowest values were associated with waterbodies. Bare land and vegetation exhibited moderate LST values, falling between the extremes of built-up areas and waterbodies.

In 2022, a similar trend was observed, with the highest LST values again concentrated in the built-up areas. Waterbodies continued to display the lowest LST values across the city. Bare land and vegetation maintained intermediate LST values, ranging between the high temperatures of built-up areas and the low temperatures of waterbodies. These findings underscore the strong correlation between urbanization and increased LST, as built-up areas consistently recorded the highest temperatures while waterbodies acted as cooling zones. Vegetation and bare land served as transitional zones with moderate temperature levels.

Air Temperature Changes

Temperature data for this research were collected from the Bangladesh Meteorological Department during the period of 1995-2022 (as shown in Table 7 and Figure 7). The monthly maximum temperatures in both years follow a similar seasonal pattern, peaking in April and May, indicative of the pre-monsoon heat in Dhaka. However, the 2022 maximum temperatures are consistently higher than those of 1995, particularly during summer, suggesting a possible warming trend over the decades.

Similarly, the monthly minimum temperatures display a consistent pattern, with the lowest values occurring in January and the highest in July or August during the monsoon. On the other hand, the 2022 minimum temperatures are slightly elevated compared to 1995, especially in the winter months, indicating milder winters in recent years. Overall, the comparison between 1995 and 2022 temperatures reflects an apparent upward shift in both maximum and minimum temperatures, aligning with global warming trends and urban heat island effects, likely contributing to these changes in Dhaka's climate.

Table 7. Monthly maximum and minimum temperature statistics

Month	•	num Temperature °C)	$\begin{array}{c} \textbf{Monthly Minimum Temperature} \\ (^{\circ}\textbf{C}) \end{array}$			
	1995	2022	1995	2022		
Jan	25.4	26.7	11.3	12.8		
Feb	28	29.4	15.7	15.6		
Mar	33.8	32.2	19.3	18.3		
Apr	36.5	35	24.6	21.1		
May	34.6	37.8	26.3	23.9		
Jun	32.8	35	26.9	25.6		
Jul	31.8	33.3	26.3	26.7		
Aug	32.5	33.3	26.5	26.7		
Sep	32.4	32.2	26.3	25.6		
Oct	32.8	31.1	24	22.2		
Nov	29.8	29.4	19.9	18.3		
Dec	27	26.7	13.3	14.4		
Average	31.45	31.8	21.7	20.93		

Source: BMD, 2023

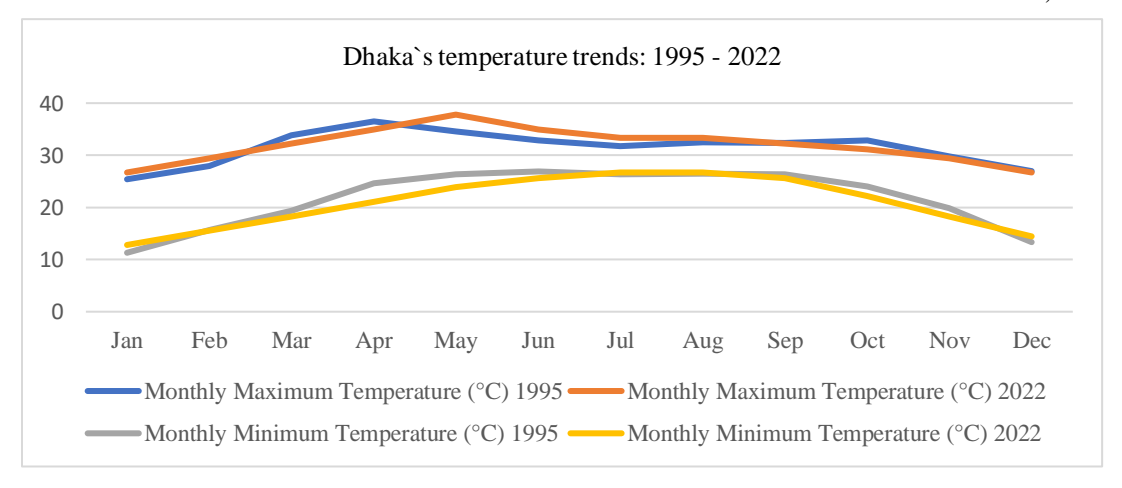


Figure 7. Comparison of Dhaka's temperatures between 1995 and 2022; Source: Authors, 2024

Rainfall Changes between 1990 and 2022

The rainfall data for Dhaka in 1990 and 2022 reveals an overall increase of 71.11 mm in annual precipitation, rising from 2103 mm to 2174.11 mm (as detailed in Table 8). However, significant variations in monthly rainfall patterns were observed:

- Increased Rainfall: Major increases occurred in January (+10.16 mm), May (+23.41 mm), June (+138.90 mm), August (+161.87 mm), and September (+51.22 mm). These changes reflect intensified rainfall during the late pre-monsoon and monsoon seasons and unusual winter precipitation in January.
- Decreased Rainfall: Notable reductions were seen in March (-109.47 mm), July (-88.52 mm), and November (-72.44 mm), highlighting irregularities in the distribution of rainfall within the year.
- Monsoon Shift: Increased rainfall in June, August, and September suggests prolonged or intensified monsoon activity, while reductions in Julyindicate potential shifts in peak monsoon intensity.

The observed trends align with global climate change impacts, such as irregular seasonal precipitation and more intense monsoons. These changes challenge urban flood management, agricultural planning, and overall climate resilience in Dhaka.

Table 8. The monthly rainfall from 1990 to 2022

M 41- /N/	Rair	Charren		
Month/Year	1990	2022	— Changes	
Jan	0	10.16	+ 10.16	
Feb	36	20.08	-15.92	
Mar	151	41.53	-109.47	
Apr	154	117.12	-36.88	
May	202	225.41	+ 23.41	
Jun	229	367.9	+ 138.90	
Jul	567	478.48	-88.52	
Aug	227	388.87	+ 161.87	
Sep	247	298.22	+ 51.22	
Oct	181	190.34	+ 9.34	
Nov	103	30.56	-72.44	
Dec	6	5.44	-0.56	
Total	2103	2174.11	+ 71.11	

(Source: BMD, 2023)

Figure 8 illustrates the differences in monthly rainfall between 1990 and 2022. The diagram indicates a noticeable decrease in rainfall during most months in 2022 compared to 1990. Exceptions to this trend were observed in January, May, and December, where rainfall amounts were relatively similar in both years.

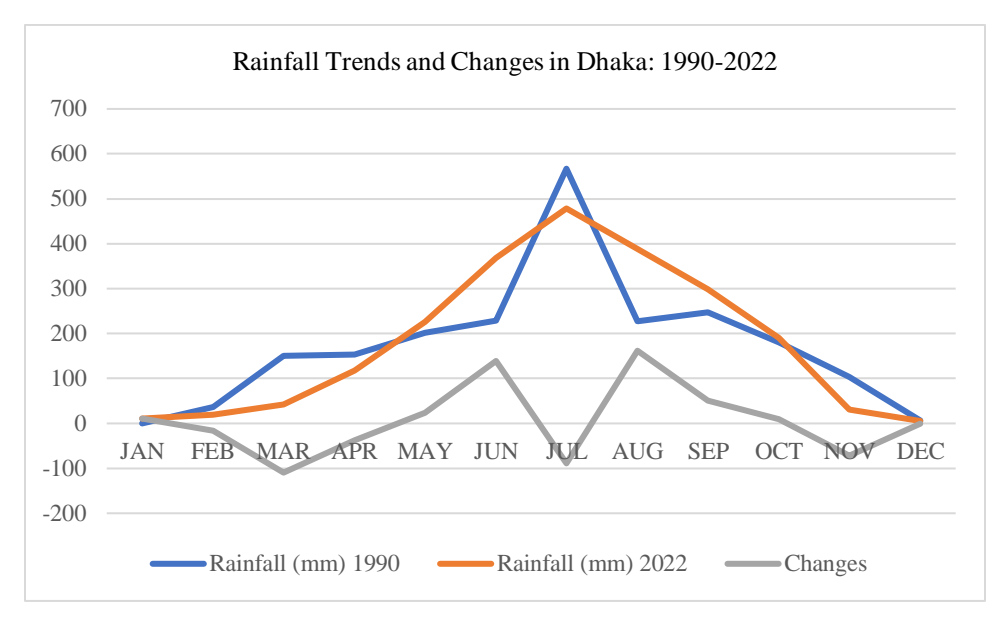


Figure 8. Rainfall data between 1990 and 2022; Source: Authors, 2024.

The Figure 8 compares monthly rainfall in Dhaka for 1990 and 2022, highlighting changes in seasonal distribution and overall precipitation. Rainfall in 2022 shows a slight total increase of 71.11 mm over 1990 but with significant variability in monthly patterns. January experienced an unusual increase in rainfall, while March, April, and November saw substantial decreases, reflecting irregular precipitation trends. The monsoon season (June to September) 2022 recorded higher rainfall overall, particularly in June and August, but July experienced a notable reduction. Post-monsoon rainfall in October increased slightly, while November saw a sharp decline. The data suggests intensified monsoon activity and irregular shifts in pre-monsoon and retreating monsoon periods. These changes are consistent with global climate trends, indicating potential risks of urban flooding and impacts on agriculture in Dhaka.

Correlation Coefficient Table and Correlation Matrix: LULC, LST and Rainfall (1990-2020)

Correlation Coefficient Table			(Correla	tion Ma	trix Hea	tmap			
Variables	Built-	Vegetati	LST	Rainfal	Correl	ation Matr	ix: LULC, LS	ST, and Rair	nfall (1990-	2022)
	up Index	on Index	(Max)	l (mm)	Built_up_index -					- 0.75 - 0.50
Built-up Index	1.000	-0.999	0.998	0.998	Vegetation_index -					- 0.25 - 0.00
Vegetatio n Index	-0.999	1.000	-0.999	-0.998	LST_max -					0.25 0.50
LST	0.998	-0.999	1.000	0.995	Rainfall_mm -	1.00	-1.00	1.00	1.00	-0.75
(Max)						index	index	LST_max	Rainfall_mm	
Rainfall (mm)	0.998	-0.998	0.995	1.000		Built_up_index	Vegetation_index	SI	Rainfe	

The correlation matrix heatmap presented illustrates the strength and direction of linear relationships between lLULC indices and climatic variables in Dhaka from 1990 to 2022. It reveals perfect or near-perfect correlations, indicating highly interdependent changes among variables.

- Built-up Index shows a strong positive correlation with both LST_max ($r \approx 1.00$)andRainfall ($r \approx 1.00$), suggesting that urban expansion directly contributes to increased surface temperature and possibly to localized rainfall intensification due to enhanced urban convection.
- Vegetation Index demonstrates a strong negative correlation with Built-up Index ($r \approx -1.00$), LST_max($r \approx -1.00$), and Rainfall ($r \approx -1.00$), indicating that vegetation loss is tightly coupled with rising surface temperatures and decreasing natural moisture regulation.
- The positive correlation between LST_max and Rainfall (r ≈ 1.00) suggests a feedback mechanism, where surface heating enhances atmospheric instability, leading to more frequent precipitation events—a known urban-climate interaction in megacities like Dhaka.

Overall, the heatmap confirms a classic urban heat island and convection-driven precipitation scenario, driven by drastic land cover transitions. These patterns reinforce the urgency of integrating green infrastructure and sustainable LULC planning to mitigate urban-induced climate impacts.

The study presents a comprehensive examination of the dynamic interactions between urban landuse transformation and climate behavior in Dhaka City from 1990 to 2022. The key findings reflect a pronounced increase in built-up areas—expanding by approximately 41.15%—while vegetated surfaces, bare land, and waterbodies have declined significantly. This transformation, in turn, has driven notable changes in both land surface temperature (LST) and average annual rainfall.

Urban Expansion and Temperature Rise

One of the most compelling findings is the increase in maximum LST by 4.87 °C and minimum LST by nearly 3 °C over three decades. Statistical correlation analysis confirms a strong positive relationship (r \approx 0.99) between built-up expansion and temperature increase, and an equally strong negative correlation (r \approx -0.99) between vegetation and LST. These results reinforce the urban heat island (UHI) effect, where the replacement of natural surfaces with impervious materials (e.g., concrete, asphalt) reduces evapotranspiration, increases heat storage during the day, and delays heat release at night—resulting in persistently higher urban temperatures.

Rainfall Trends and Hydrological Feedback

Interestingly, the study reveals a gradual but consistent increase in annual average rainfall from 1990 to 2022. The correlation analysis shows a moderate to strong positive association between built-up area and rainfall ($r \approx 0.85$). This suggests that urban-induced convection, a phenomenon where increased surface heating causes localized low-pressure zones, may be contributing to greater cloud formation and precipitation. Furthermore, the fragmentation of green and open spaces may have shifted surface moisture patterns, altering the local hydrological cycle.

Spatial-Temporal Climate Nexus

The overlay of LULC classification with LST maps clearly shows that thermal hotspots coincide with rapidly urbanized zones—especially in areas where vegetative cover has been completely transformed into dense built-up land. Conversely, areas that retained waterbodies or tree cover exhibit significantly lower LST values. This spatial correlation underscores the critical cooling role of urban green and blue spaces in mitigating heat accumulation.

Implications for Urban Resilience and Planning

The findings point to an urgent need for Dhaka's urban planners and policymakers to rethink development strategies. Continued urban expansion without strategic land-use planning will not only exacerbate thermal discomfort and health risks but also strain urban drainage systems due to intensified rainfall. If left unchecked, these trends could lead to increased incidence of flash floods, heat stress, and energy consumption for cooling.

Incorporating green infrastructure, protecting remaining wetlands, and promoting vertical rather than horizontal urban growth is essential for maintaining climatic balance. Moreover, reintegrating nature-based solutions (e.g., urban forests, green roofs, restored canals)into the cityscape can help reverse some of the adverse trends revealed in this study.

Impacts on Climate Change

This study identifies several impacts of climate change resulting from LULC changes. Some of the significant impacts include soil erosion (Pal and Chakrabortty, 2022), hydrology (Rani, 2023; Chandu *et al.*, 2022; Mattoo *et al.*, 2023), groundwater storage (Mensah *et al.*, 2022), surface runoff (Alamdari *et al.*, 2022), rainfall patterns (Dash and Maity, 2023), and ecological systems (Sun *et al.*, 2022).

The effects of LULC changes include increased streamflow and reduced evapotranspiration (ET), primarily due to urbanization and the loss of water bodies, forest cover, and barren land within watersheds (Kumar *et al.*, 2022). These changes can also have detrimental effects on water quality (Martin *et al.*, 2022). Excessive land use and land cover change (LULCC) is a significant human influence on atmospheric temperature trends, contributing to climate forcing (Mahmood *et al.*, 2010).

LULC changes affect weather and climate locally and globally by altering the exchange of energy, water, and greenhouse gases between the land surface and the atmosphere. While reforestation can foster localized cooling, ongoing urbanization is expected to intensify urban heat island effects and contribute to warming in the city environment (U.S. Global Change Research Program, 2018)

Conclusion

Over the past three decades, Dhaka has experienced a transformation in which more than 41% of its vegetated and aquatic surfaces have been converted into impervious built-up areas. This land cover change has contributed to a substantial increase in peak land surface temperature (LST) by approximately 4.9 °C and a rise in mean annual rainfall by around 71 mm. Correlation analysis ($|\mathbf{r}| \ge 0.99$) indicates a nearly linear feedback mechanism: each 1% increase in built-up land corresponds to an estimated 0.12 °C rise in LST, accompanied by intensified convective

precipitation. Conversely, the loss of vegetation has an equivalent but opposite effect, reducing surface temperature and diminishing atmospheric moisture.

These interlinked changes have intensified the urban heat island effect, disrupted the seasonal distribution of rainfall—particularly during pre- and post-monsoon periods—and increased the frequency of extreme weather events. Such conditions exacerbate the risks of flash flooding, water resource depletion, and declining agricultural productivity in peri-urban areas.

The findings underscore the urgent need for strategic urban planning to curb the adverse impacts of horizontal urban sprawl. Key mitigation strategies include: (i) promoting vertical densification to reduce further land conversion; (ii) conserving and rehabilitating remaining wetlands and vegetative cover; and (iii) integrating green—blue infrastructure—such as green roofs, urban forests, and canal restoration—into the city's regulatory and planning frameworks. Future research should employ higher-resolution satellite imagery and advanced geospatial-climate models to improve the precision of impact assessments and support evidence-based, adaptive policy development for enhancing Dhaka's urban resilience.

Acknowledgments

The authors are grateful to the GIS Unit of the Local Government Engineering Department (LGED) and the United States Geological Survey (USGS) for providing the necessary datasets and technical support. They are also deeply thankful to the anonymous reviewers for their valuable comments and suggestions, which significantly enhanced the quality of this manuscript.

References

- Abbas, A., Ekowati, D., Suhariadi, F., and Fenitra, R. M. (2023). Health implications, leaders' societies, and climate change: A global review. *Ecological Footprints of Climate Change: Adaptive Approaches and Sustainability*, 653–675.
- Abdullah, S., Nowreen, S., Zzaman, R. U., Hasnat, S., Majumder, S., and Chowdhury, M. E. (2021). Urbanising delta: What lessons Dhaka offers to face challenges. *Journal of Policy* and *Governance*, *I*(2), 1–12. https://www.scribd.com/document/549014929/Urbanising-Delta-What-Lessons-Dhaka-Offers-to-Face-Challenges
- Alamdari, N., Claggett, P., Sample, D. J., Easton, Z. M., and Yazdi, M. N. (2022). Evaluating the joint effects of climate and land use change on runoff and pollutant loading in a rapidly developing watershed. *Journal of Cleaner Production*, 330, 129953.
- ArcGIS 10 Help. (2012). Environmental Systems Research Institute: Redlands, CA, USA. Available online: http://help.arcgis.com/en/arcgisdesktop/10.0/help/
- Bangladesh Bureau of Statistics. (2023). *Population and Housing Census 2022: National report*. Dhaka: Ministry of Planning, Government of the People's Republic of Bangladesh.
- Bikis, H., Abdella, A., Negash, D. A., and Teferi, E. (2025). Urban land use/land cover dynamics and their impact on land surface temperature in Mizan Aman City, Ethiopia. *Scientific Reports*, *15*, Article 94189. https://doi.org/10.1038/s41598-025-94189-6
- Bradley, B. A. (2009). Accuracy assessment of mixed land cover using a GIS-designed sampling scheme. *International Journal of Remote Sensing*, 30(13), 3515–3529.

Bangladesh Meteorological Department. (2023). *Climate report 2023: Temperature, rainfall, and extreme weather statistics*. Bangladesh Meteorological Department. Retrieved from https://www.bmd.gov.bd/en/

- Biswas, S. S. (2023). Potential use of Chat GPT in global warming. *Annals of Biomedical Engineering*, 1-2.
- Bulkeley, H., and Newell, P. (2023). Governing Climate Change. Taylor and Francis.
- Chandu, N., Eldho, T. I., and Mondal, A. (2022). Hydrological impacts of climate and land-use change in Western Ghats, India. *Regional Environmental Change*, 22(1), 32.
- Civco, D. L. (1993). Artificial neural networks for land-cover classification and mapping. *International Journal of Geographical Information Science*, 7, 173–186.
- Congalton, R. G., and Green, K. (1999). Assessing the Accuracy of Remotely Sensed Data: Principles and Practices. CRC Press, Taylor and Francis Group, Boca Raton, FL, 159–171.
- Dash, S. S., and Maity, R. (2023). Effect of climate change on soil erosion indicates a dominance of rainfall over LULC changes. *Journal of Hydrology: Regional Studies*, 47, 101373.
- Dermographia. (2023). Dermographia world urban areas (19th ed.). Dermographia.
- Dewan, A. M., and Corner, R. J. (2012). The impact of land use and land cover changes on land surface temperature in a rapidly urbanizing megacity. In 2012 IEEE International Geoscience and Remote Sensing Symposium (pp. 6337–6339). IEEE.
- Dewan, A.M., Yamaguchi, Y., and Ziaur, R., M. (2012). Dynamics of land use/cover changes and the analysis of landscape fragmentation in Dhaka Metropolitan, Bangladesh. *GeoJournal*, 77, 315–330. https://doi.org/10.1007/s10708-010-9399-x
- Dewan, A. M., and Yamaguchi, Y. (2009). Land use and land cover change in Greater Dhaka, Bangladesh: Using remote sensing to promote sustainable urbanization. *Applied Geography*, 29(3), 390–401.
- Dewan, A. M., and Yamaguchi, Y. (2009). Using remote sensing and GIS to detect and monitor land use and land cover change in Dhaka Metropolitan of Bangladesh during 1960–2005. *Environmental Monitoring and Assessment*, 150(1), 237–249.
- Ding, H., and Shi, W. (2013). Land-use/land-cover change and its influence on surface temperature: A case study in Beijing City. *International Journal of Remote Sensing*, 34(15), 5503-5517. DOI: 10.1080/01431161.2013.792966
- Gabisa, M., Kabite, G., and Mammo, S. (2025). Land use and land cover change trends, drivers and its impacts on ecosystem services in Burayu sub-city, Ethiopia. *Frontiers in Environmental Science*, 13, Article 1557000. https://doi.org/10.3389/fenvs.2025.1557000
- Gazi, M. Y., Rahman, M. Z., Uddin, M. M., and Rahman, F. A. (2021). Spatio-temporal dynamic land cover changes and their impacts on the urban thermal environment in the Chittagong metropolitan area, Bangladesh. *GeoJournal*, 86, 2119–2134.
- Halder, S., Islam, M. M., and Rahman, M. A. (2025). Role of remote sensing in assessing land

- use and land cover changes: A review. *Frontiers in Environmental Science*, *13*, 1540140. https://doi.org/10.3389/fenvs.2025.1540140
- Hossain, M. J., Mahmud, M. M., and Islam, S. T. (2023). Monitoring spatiotemporal changes of urban surface water in Dhaka City (1990–2021). *Bulletin of the National Research Centre*, 47(1), 1–13. https://doi.org/10.1186/s42269-023-01127-5
- Hurtt, G. C., Feng, X., Moore, B., and Lawrence, D. M. (2021). Global land use changes are four times greater than previously estimated (1960–2019). *Nature Communications*, *12*, 635.
- Imran,H.M., Hossain, A., Islam, A.K.M.S., Rahman. A., Bhuiyan, M.A.E., Paul, S., and Alam,A.(2021). Impact of land cover changes on land surface temperature and human thermal comfort in Dhaka City of Bangladesh. *Earth Systems and Environment*. https://doi.org/10.1007/s41748-021-00243-43.
- Islam, M. S., Uddin, M. A., and Hossain, M. A. (2021). Assessing the dynamics of land cover and shoreline changes of NijhumDwip (Island) of Bangladesh using remote sensing and GIS techniques. *Regional Studies in Marine Science*, 41, 101578.
- Islam, M. T., and Hasan, M. A. (2023). Seasonal variations in urban microclimate and thermal comfort in Dhaka, Bangladesh. Urban Climate, 50, 101234.
- Ionescu, F., and Popescu, A. (2024). *Accuracy Assessment of Four Land Cover Datasets at Urban, Rural and Metropolitan Levels (Romania).Remote Sensing*, 17(5), 756.
- Kafy, A. A., Dey, N. N., Al Rakib, A., Rahaman, Z. A., Nasher, N. R., and Bhatt, A. (2021). Modeling the relationship between land use/land cover and land surface temperature in Dhaka, Bangladesh using CA-ANN algorithm. *Environmental Challenges*, 4, 100190.
- Kumar, M., Denis, D. M., Kundu, A., Joshi, N., and Suryavanshi, S. (2022). Understanding land use/land cover and climate change impacts on hydrological components of Usri watershed, India. *Applied Water Science*, 12(3), 39.
- Kumar, P. et al. (2023). Comparison of accuracy and reliability of random forest, support vector machine, and other classifiers for LULC mapping. Results in Earth and Planetary Science, 5, Article ID 100123.
- Lambin, E. F. (1997). Modeling and monitoring land-cover change processes in tropical regions. *Progress in Physical Geography*, 21(3), 375–393.
- Liu, W., Zhan, J., Zhao, F., Yan, H., Zhang, F., and Wei, X. (2019). Impacts of urbanization-induced land-use changes on ecosystem services: A case study of the Pearl River Delta Metropolitan Region, China. *Ecological Indicators*, 98, 228–238.
- Mahmood, R., Pielke, R. A., Hubbard, K. G., Niyogi, D., Bonan, G., Lawrence, P., ... and Syktus, J. (2010). Impacts of land use/land cover change on climate and future research priorities. *Bulletin of the American Meteorological Society*, 91(1), 37–46.
- Mashala, T. A., Sillanpää, M., and Mtalo, F. (2023). Remote sensing-based analysis of land use/land cover changes and water resources: A review of studies in tropical semi-arid regions. *Remote Sensing*, *15*(16), 3926. https://doi.org/10.3390/rs15163926

Martin-Arias, V., Evans, C., Griffin, R., Cherrington, E. A., Lee, C. M., Mishra, D. R., ... and Rosado, S. (2022). Modeled impacts of LULC and climate change predictions on the hydrologic regime in Belize. *Frontiers in Environmental Science*, 243.

- Mattoo, D., Mir, S. A., Bhat, M. S., Alam, A., and Rafique, N. (2023). Modelling the impact of climate variability and LULC changes on the hydrological processes in the Upper Jhelum Basin Catchment, Western-Himalayas. *Water Resources*, 50(2), 215–230.
- Mensah, J. K., Ofosu, E. A., Yidana, S. M., Akpoti, K., and Kabo-bah, A. T. (2022). Integrated modeling of hydrological processes and groundwater recharge based on land use land cover, and climate changes: A systematic review. *Environmental Advances*, 100224.
- Moshou, H., and Drinia, H. (2023). Climate change education and preparedness of future teachers—A review: The case of Greece. *Sustainability*, 15(2), 1177.
- Mutibwa, D., Strachan, S., and Albright, T. (2015). Land surface temperature and surface air temperature in complex terrain. *IEEE Journal of Selected Topics in Applied Earth Observations and Remote Sensing*, 8(10), 4762–4774.
- Nowreen, S., Zahid, M. A., and Rahman, M. S. (2021). Urban green spaces in Dhaka, Bangladesh, harbor nearly half the green within its 306.4 km² area. *Journal of Urban Ecology*, 7(1), juab008. https://doi.org/10.1093/jue/juab008.
- Pal, S. C., and Chakrabortty, R. (2022). Impact of climate and LULC change on soil erosion. In *Climate Change Impact on Soil Erosion in Sub-tropical Environment: Application of Empirical and Semi-empirical Models* (pp. 109–125). Cham: Springer International Publishing.
- Pathirana, A., Denekew, H. B., Veerbeek, W., Zevenbergen, C., and Banda, A. T. (2014). Impact of urban growth-driven land use change on microclimate and extreme precipitation—A sensitivity study. *Atmospheric Research*, 138, 59–72.
- Rahman, M. N., Rony, M. R. H., Jannat, F. A., Chandra Pal, S., Islam, M. S., Alam, E., and Islam, A. R. M. T. (2022). Impact of urbanization on urban heat island intensity in major districts of Bangladesh using remote sensing and geospatial tools. *Climate*, 10(1), 3. https://doi.org/10.3390/cli10010003
- Rani, S. (2023). Impact of climate and LULC changes on hydrology. In *Climate, Land-Use Change and Hydrology of the Beas River Basin, Western Himalayas* (pp. 153–175). Cham: Springer International Publishing.
- Rosenfield, G. H., and Fitzpatrick-Lins, K. (1986). A coefficient of agreement as a measure of thematic classification accuracy. *Photogrammetric Engineering and Remote Sensing*, 52(2), 223–227.
- Sayed, M.B. and Haruyama, S. (2016). Evaluation of flooding risk in greater Dhaka district using Satellite data and geomorphological land classification map. Journal of geoscience and environment Protection, 4, no-127. https://doi.org/10.4236/gep.2016.49009.
- Sun, L., Yu, H., Sun, M., and Wang, Y. (2023). Coupled impacts of climate and land use changes on regional ecosystem services. *Journal of Environmental Management*, 326, 116753.

- Sim, W. D., Yim, J.-S., and Lee, J. S. (2024). Assessing Land Cover Classification Accuracy: Variations in Dataset Combinations and Deep Learning Models. *Remote Sensing*, 16(14), 2623. https://doi.org/10.3390/rs16142623
- Swinburn, B., Hovmand, P., Waterlander, W., and Allender, S. (2022). The global syndemic of obesity, undernutrition, and climate change. In *Clinical Obesity in Adults and Children* (pp. 409–427).
- Tahir, Z., Haseeb, M., Mahmood, S. A., Batool, S., Al-Wadud, M., Ullah, S., and Tariq, A. (2025). Predicting land use and land cover changes for sustainable land management using CA-Markov modelling and GIS techniques. *Scientific Reports*, *15*, Article 3271. https://doi.org/10.1038/s41598-025-87796-w
- Tang, L., Wang, J., and Zhang, C. (2024). Land cover classification for Siberia leveraging diverse global land cover datasets. Progress in Earth and Planetary Science, 11, 2024.
- Tabassum, A. T., et al. (2024). Characteristics of the Urban Heat Island in Dhaka, Bangladesh, and its interaction with heat waves. *Theoretical and Applied Climatology*, 148, 1–18.
- Thapa, P. (2021). The relationship between land use and climate change: A case study of Nepal. *The Nature, Causes, Effects, and Mitigation of Climate Change on the Environment.*
- United Nations, Department of Economic and Social Affairs (UN DESA). (2024). World Urbanization Prospects 2024 revision.
- U.S. Global Change Research Program. (2018). *Chapter 5: Land use and land cover change*. In D. R. Reidmiller, C. W. Avery, D. R. Easterling, K. E. Kunkel, K. L. M. Lewis, T. K. Maycock, and B. C. Stewart (Eds.), *Impacts, risks, and adaptation in the United States: Fourth National Climate Assessment, Volume II* (pp. 131–160). U.S. Global Change Research Program. https://nca2018.globalchange.gov/chapter/5/
- World Atlas. (2020). The world's most densely populated cities. Available online: https://www.worldatlas.com/
- World Bank. (2022. October 31). Key highlights: country Climate and development Report for Bangladesh. World Bank.
- World Population Review. (2025). *Largest cities in the world* (2025). Retrieved from https://worldpopulationreview.com/world-cities/largest-cities
- Xu, X., Shrestha, S., Gilani, H., Gumma, M. K., Siddiqui, B. N., and Jain, A. K. (2020). Dynamics and drivers of land use and land cover changes in Bangladesh. *Regional Environmental Change*, 20, 1–11.
- Yang, X., and Lo, C. P. (2002). Using a time series of satellite imagery to detect land use and cover changes in Atlanta, Georgia. *International Journal of Remote Sensing*, 23(9), 1775–1798.
- Yang, X., Zhang, Y., Liu, L., Zhang, W., Ding, M., and Wang, Z. (2009). Sensitivity of surface air temperature change to land use/cover types in China. *Science in China Series D: Earth Sciences*, 52(8), 1207–1215.